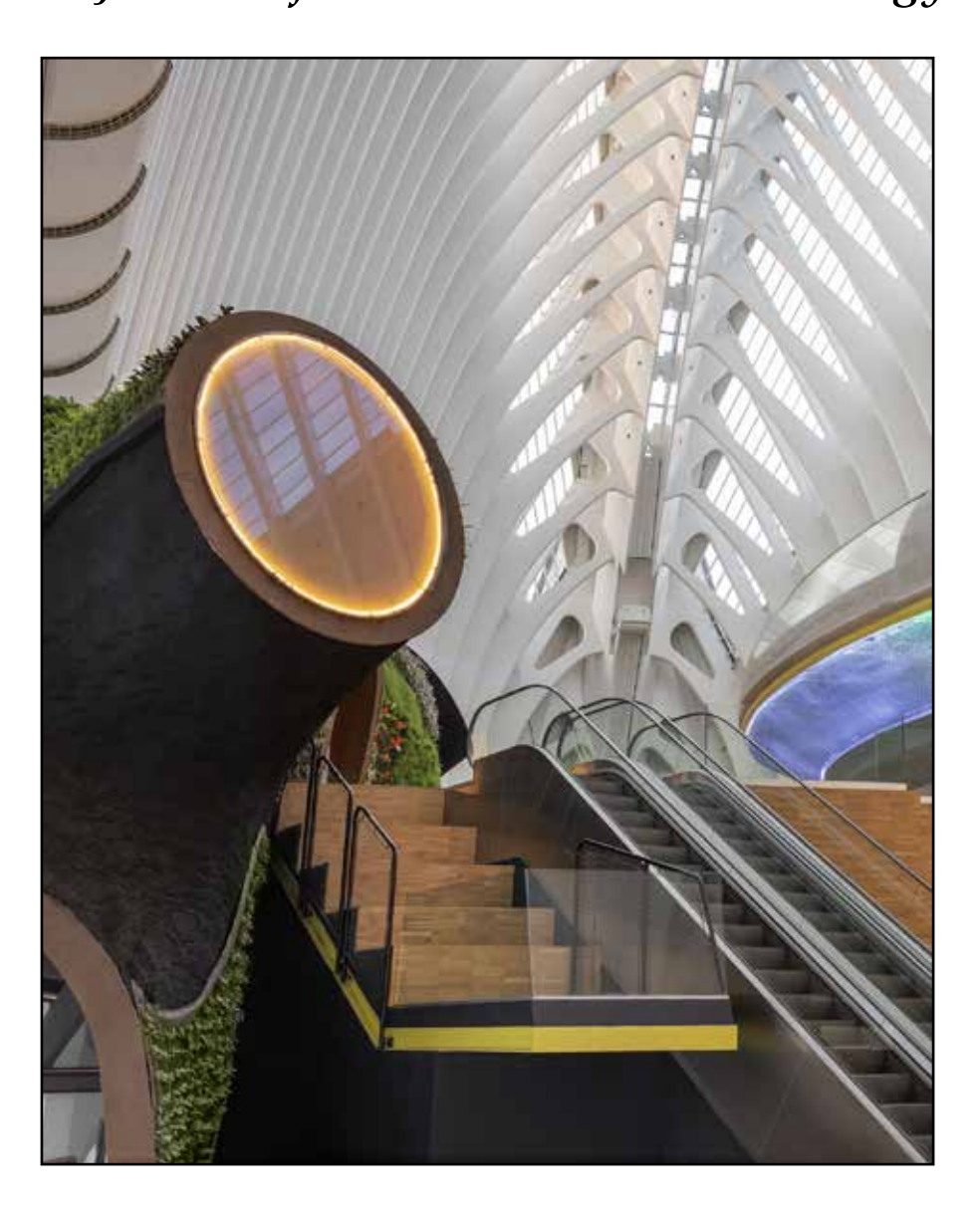
2023 Volume 64 Number 2

GLASS TECHNOLOGY

European Journal of Glass Science and Technology Part A









The European Journal of Glass Science and Technology is a publishing partnership between the Deutsche Glastechnische Gesellschaft and the Society of Glass Technology. Manuscript submissions can be made through Editorial Manager, see the inside back cover for more details.

Senior Editor

Professor Alastair Cormack **Regional Editors** Professor C. Roos Professor J. M. Parker Professor A. Duran Professor Bo Ionson Dr A. C. Hannon Professor M. Liška Professor Y. Yue Professor R. J. Hand

Managing Editor D. Moore **Assistant Editor** S. Lindley

Society of Glass Technology 9 Churchill Way Chapeltown Sheffield S35 2PY, UK +44(0)114 263 4455 Email info@sgt.org
Web http://www.sgt.org

The Society of Glass Technology is a registered charity no. 237438.

Advertising Requests for display rates, space orders or editorial can be obtained from the above address.

Glass Technology: European Journal of Glass Science and Technology, Part A ISSN 1753-3546 (Print) ISSN 1753-3554 (Online)

The journal is published six times a year at the beginning of alternate months from February.

Electronic journals: peer reviewed papers can be viewed by subscribers through Ingenta http://www.ingentaconnect.com

The editorial contents are the copyright

Claims for free replacement of missing journals will not be considered unless they are received within six months of the publication date.

Volume 64 Number 2

Glass Technology

European Journal of Glass Science and Technology A

CONTENTS

- 33 Know Your Furnace: furnace maintenance including electric boost Stuart Hakes
- 42 Alfred University developing robust concrete fortified with recycled waste
- 43 Piecing together Scotland's religious past with shards of glass
- 45 News
- 54 Conferences and events
- 57 Semiconducting and scintillating glasses for x-ray detection B. Smith, J. Mucciaccio, T. Caplice, L. Wadle, L. McClanahan, L. G. Jacobsohn & U. Akgun

Cover: La Caixa Foundation Cultural Center, built by Acsa Sorigué, designed by architect Enric Ruiz-Geli, Cloud9. The project has been designed to give life within the iconic building of the Agora. A series of capsules or "living cells" make up a futuristic landscape that appears as a public square with oak bleachers with an auditorium below, two exhibition halls, a restaurant, the VIP area and the administration area, a bookstore and a more unique element, in the center, which represents a cloud. Vidres Berni has participated in all the different glass installations: access façade, mirror cladding, railings and laminar glass closures, coatings with coloured glass, oculi of the restaurant, etc. © Miguel Lorenzo

This publication is brought to you in part by support from

Darshana and Arun Varshneya (Hon.FSGT)

of

Saxon Glass Technologies, Inc., Alfred NY

"To promote the R&D in glass science, engineering, and technology across the globe"

"To disseminate such knowledge to human society-at-large"

Semiconducting and scintillating glasses for x-ray detection

B. Smith, J. Mucciaccio, T. Caplice, L. Wadle, L. McClanahan, L. G. Jacobsohn & U. Akgun^{1,*}

Received 14 April 2022 Revision received 11 Feb 2023 Accepted 13 Feb 2023

X-ray detectors are commonly used for medical, crystallography and space physics applications. Most of the current x-ray detectors use cadmium zinc telluride (CZT) as the active medium. This report investigates high density semiconducting and scintillating glasses as potential alternatives to CZT. For the semiconducting glasses, samples composed of $xCuO-((1-x)/2)PbO-((1-x)/2)V_2O_5$ and $xFeO-((1-x)/2)PbO-((1-x)/2)V_2O_5$, for the scintillating glasses, samples composed of $xGd_2O_3+yWO_3+(1-x-y)2H_3BO_3$, doped with 1-6% Eu³⁺ or Tb³⁺, were investigated in this study. The glass-making conditions, density, Raman spectroscopy analysis, photoluminescence excitation and emission spectra, as well as conductivity measurements performed on various samples, are reported. The interaction of x-rays with all the glass samples was simulated using GATE software, and their mass attenuation coefficients were calculated and compared with CZT.

Introduction

X-ray detection, and the development of materials for x-ray detectors, are strategic areas of interest. (1) The applications of x-rays are widespread; (2,3) however, several factors limit the effectiveness of various materials such as x-ray sensors. Sensor materials should provide good energy resolution and high spatial resolution while having a high effective atomic number ($Z_{\rm eff}$) and high mass attenuation coefficients for efficient x-ray detection. (2) Finally, many sensors are constrained by manufacturing limitations regarding the ease of bulk production and the cost of material components. Almost all x-ray detectors use either semiconducting or scintillating active media. This work investigates the use of glass as a competitive solution in both categories.

The most commonly used detector material for medical imaging is cadmium zinc telluride (CZT). (4-6) This is due to its high density, high effective atomic number and high mass attenuation; as well as its excellent performance at room temperature. (6-8) However, the mass production of CZT, being a crystalline material, has some difficulties, such as high costs, low production yields, and extensive production time. (4,7-10) Several glasses offer properties that make them potential alternatives to CZT as the active material in x-ray detectors. (11-16) The main advantage of these glasses is that they directly address the manufacturing problems of CZT; specifically, ease of production, mouldability, low manufacturing cost and low manufacturing time. (17,18)

This investigation focuses on two types of glasses

to be used as convenient alternatives to CZT as x-ray detector materials. The first type of glass is lead vanadate, doped with iron and copper, for use as a semiconductor detector. Semiconductor detectors respond to incident radiation by exciting electrons from the valence band to the conduction band, creating electron—hole pairs, which can be used to produce an electric signal. The intensity of the electrical signal is related to the energy of the x-ray. The second type of glass is gadolinium borotungstate doped with europium or terbium 3+ions which act as scintillating agents; scintillator-based detectors utilize optical signals to detect x-rays. In this case, the intensity of the light, transformed into an electrical signal by the photodetector is related to the energy of the x-ray.

The semiconducting glasses were chosen for their high density, high effective atomic number, bandgap and charge carrier mobility. Iron and copper were chosen for dopants because of their ability to create mixed-valence states when in glass, making them ideal for increasing small polaron hopping, (21,22) a feature already present in vanadate glasses. (23,24) In this report, we investigate the changes in the electrical properties of these glasses as the concentrations of the dopants increase.

The scintillating glasses were chosen for their high density, high effective atomic number, and optical transparency to scintillation emission. (11) Europium and terbium were chosen as dopants because their emission wavelengths match the sensitivity of commercial photodetectors (8,12,14) and they are easy to integrate into the glass systems of interest.

There have been many recent developments in the use of glass-based particle detectors. Radioluminescence measurements have previously evaluated high

¹ Physics Department, Coe College, Cedar Rapids, IA, USA

² Department of Materials Science and Engineering, Clemson University, Clemson, SC, USA

 $^{^{\}ast}$ Corresponding author. Email uakgun@coe.edu DOI: 10.13036/17533546.64.2.04

Semiconducting (e) Fe_2O_3 CuO PbO V_2O_5 T_g (°C) Density (g/cm³) Glass e0 0 0.5 0.5 256 5.4 48.76 Glass e1 0.010.4950.495255 5.4 48.500 Glass e2 0.025 0 0.48750.4875276 5.3 48.11Glass e3 0.050 0.450.45281 5.3 45.02 Glass e4 0.10 0.450.45287 5.2 46.15Glass e5 0.2 0.40.4287 5.1 43.540 Glass e6 0 0.010.4950.495246 5.4 48.54 0 0.025 0.48750.4875250 5.3 48.21Glass e7 Glass e8 0 0.050.4750.475256 5.2 47.65 Glass e9 0 0.10.450.45256 5.2 46.55 Glass e10 0 0.2 0.40.4256 5.1 44.33

231

Table 1. Semiconducting glasses - chemical composition (by molar fractions) and properties

0.35

0.35

density $Sm^{\scriptscriptstyle 3+}$ and $Ce^{\scriptscriptstyle 3+}$ doped glasses. $^{\scriptscriptstyle (12,25,26)}$ It has been reported that nanoparticles in glass ceramics improve spatial resolution in digital radiography. (27) Similar research has also sought to make fluoride glass calorimeters for use in the Large Hadron Collider. (28) These results can be easily adapted to make a smaller detector suitable for medical x-ray imaging. Similar materials can be used for proton detection, (29,30) and improved with artificial intelligence (AI) to make them even more effective than current x-ray radiation therapy for cancer. (31,32) A similar approach of scintillating glass and machine learning can also be used for neutron detection. (33) Lead vanadate-based semiconducting glasses have been previously used, by the author of this study, in resistive plate chamber detectors designed for high energy physics experiments.(34)

This work focuses on developing copper or irondoped lead-vanadate semiconducting glasses, as well as europium or terbium-doped gadolinium and tungsten-based scintillating glasses for x-ray detectors in various applications.

Methods

Glass e11

0

Both semiconducting and scintillating glass samples were prepared using powdered chemicals of reagent grade purity or higher. Semiconducting reagents and their relative amounts are reported in Table 1 by molar fractions. The formulas used for the semiconducting glasses were xCuO-((1-x)/2)PbO-((1-x)/2) $V_2\text{O}_5$ and $x\text{FeO-}((1-x)/2)\text{PbO-}((1-x)/2)\text{V}_2\text{O}_5$. These compounds were combined in alumina crucibles and manually mixed for 5 min to ensure homogeneity. The samples were heated in a furnace at temperatures ranging from 900 to 1000°C for 10 to 20 min. The samples were poured on a steel plate or a graphite mould, to be quenched at room temperature.

The compounds and their relative ratios used for the scintillating glasses are reported in Table 2. The formula used for the scintillating glasses was $xGd_2O_3+yWO_3+(1-x-y)2H_3BO_3$. Rare earth compounds in the form of Eu_2O_3 and Tb_2O_3 , were added in excess to the glass mixtures ranging from 1 to 6 mol%. Similarly, the reagents were manually mixed in alumina crucibles for 5 min to ensure homogeneity. The samples were heated in a furnace for 30 min at 1200°C. The melted samples were then poured onto a

steel plate. In both cases, the crucibles were weighed partway through melting to ensure the expected weight loss.

The glass transition temperature (T_g) was determined in two different ways. The T_g of the semiconducting glass samples was measured using a TA Instruments Q200 differential scanning calorimeter (DSC), and the T_g of the scintillating glass samples was measured using a PerkinElmer simultaneous thermal analyzer (STA) 6000. Density measurements were performed using a Quanta Chrome micro-ultra pycnometer 1000. A Keithly 6517B electrometer was used for the DC resistivity values of the semiconducting glasses. Gold sputtering was used to create electrodes on either side of the sample, and an adjustable 1000 V power supply was used during the resistivity measurements. The top surface of the glass samples was first surrounded with a gold guard to prevent interference with surface conductivity and secured with copper tape. The bottom of the sample was then secured with copper tape onto a brass plate. Electrodes were then attached and the electrometer settings were arranged to ensure isotropic behaviour in the sample. The whole setup was electrically shielded and monitored with an oscilloscope.

The mass attenuation coefficients were calculated for the various glasses using data from simulations performed with GATE software. (35) GATE (36) is an opensource, Monte-Carlo simulation kit designed for medical physicists, utilizing the most common open-source particle physics simulation software GEANT4. (37) GATE provides well-validated physics models, sophisticated geometry descriptions, and powerful visualization and 3D rendering tools with the original features specific to emission tomography. Studies show accuracy finer than 2% can easily be achieved for the passage of particles through matter. (35) The simulations reported here utilized GATE's standard EM Physics package in all simulations. The simulated setup consisted of a 0.01 mm sample of the material in front of a gamma beam with a lead block behind it. The sample had to be this thin to achieve a measurable transmission of low-energy electromagnetic radiation. The mass attenuation coefficients were calculated using the Beer-Lambert law, $I(x)=I_0e^{-\mu x}$, where I(x) is the intensity of the beam at depth x, μ is the linear attenuation coefficient, and *x* is the thickness of the absorbing material. The

Table 2. Scintillating glass bases: chemical composition (by molar fractions) and properties

Scintillating		T_{g}	Density			
(c)	Gd_2O_3	WO_3	$2H_3BO_3$	(°C)	(g/cm³)	$Z_{\it eff}$
Glass c1	0.20	0.20	0.60	724	5.17	29.81
Glass c2	0.25	0.25	0.50	689	5.26	35.42
Glass c3	0.25	0.35	0.40	664	5.54	41.37
Glass c4	0.25	0.45	0.30	649	6.15	47.31

intensity of the beam was measured in terms of the number of incoming photons, and I(x) is the number of particles that passed through the x thickness of an absorber without interacting at all. Mass attenuation coefficients are energy-dependent; therefore, the simulation was run for a range of energies from 0.01 MeV to 20 MeV. The results were compared to the mass attenuation coefficients reported by NIST for water. (38)

The $Z_{\rm eff}$ values of the glasses reported in Tables 1 and 2 were calculated using the power law for compounds, which depends on the fraction of the total number of electrons and the atomic number for each element. The $Z_{\rm eff}$ for each compound used was calculated and then a weighted average of these values was used to determine the $Z_{\rm eff}$ of each glass.

Photoluminescence emission (PL) and excitation (PLE) measurements were obtained using a Jobin Yvon Horiba Fluorolog 3 spectrophotometer equipped with a 450 W Xe lamp for excitation. A dedicated monochromator was used to select desired excitation wavelength from the Xe lamp source, and another dedicated monochromator was used to select desired emission wavelength for measurement. The number of detected photons was automatically corrected by the instrument's software for the background and spectral differences in excitation intensity and detection sensitivity. Emission and excitation spectra were acquired by scanning at the glass's peak excitation and emission wavelengths, respectively. For Eu-doped glasses, excitation measurements were set at 394 nm, and emission measurements were set at 613 nm. For Tb-doped glasses, these values were 378 nm and 542 nm, respectively.

Raman Spectroscopy was performed only on scintillating glasses using a JASCO NRS 3100 micro-Raman spectrophotometer with a 785 nm laser. Measurements were taken with a 50× magnification lens, using two acquisitions that lasted 30 s each.

Results and discussion

As previously mentioned, the goal of this study is to find a viable glass replacement for CZT-based x-ray detectors. To maximize the interactions with the x-rays the material should have a high mass density, high $Z_{\rm eff}$, and high mass attenuation coefficient. These variables are all related to each other and are used to compare the materials. Table 1 and Table 2 list the density and $Z_{\rm eff}$ values for the glass samples prepared for this work. Figure 1 demonstrates that the density of the scintillating glasses mainly depends

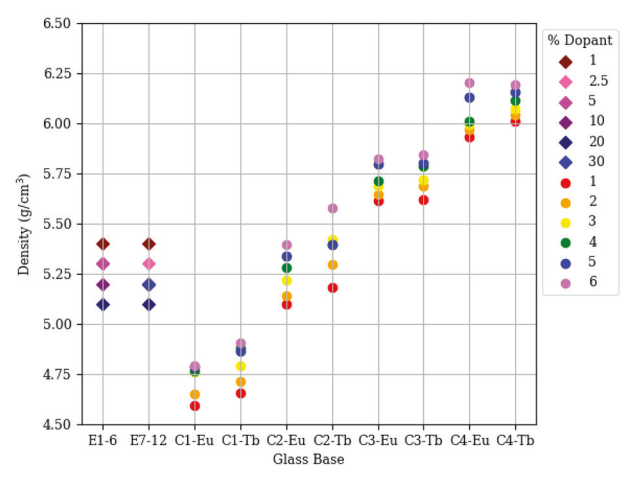


Figure 1. Density of glasses in g/cm³ organized by glass and dopant concentration. Diamonds labelled E1-5 and E6-11 correlate to the semiconducting glasses, whereas circles labelled C1-Eu through C4-Tb correlate to the scintillating glasses. Eu and Tb in the labels of scintillating glasses C1 through C4 represent the dopants within the glass samples [Colour available online]

on the tungsten concentration and varies between 4·5 and 6·3 g/cm³, with slightly higher densities for the higher Eu and Tb concentrations. The semiconducting glasses have less density variation despite the greater dopant concentration range, with values between 5·1 and 5·4 g/cm³. Interestingly, the density of the semiconducting glasses decreased for higher dopant concentrations. Overall, these density values are comparable, and in some cases superior, to the CZT density (5·68 g/cm³).⁽⁶⁾

Figure 2 shows that the scintillating glasses can reach up to $Z_{\rm eff}$ =47·3 with 45% tungsten concentration and go down to $Z_{\rm eff}$ =30 with 20% tungsten concentration. Similar to the density variation, the semiconductive glasses show less variation in their $Z_{\rm eff}$ values. The samples with the highest lead concentrations reach up to $Z_{\rm eff}$ =48 while the lowest lead concentrations go down to $Z_{\rm eff}$ =42. Especially, the

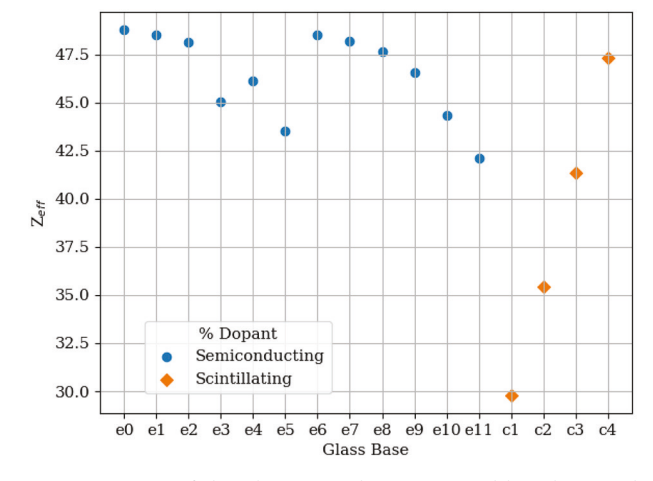


Figure 2. $Z_{\rm eff}$ of the glass samples organized by glass and dopant concentration. Blue circles labelled e0–e11 correlate to the semiconducting glasses, whereas the orange diamond labels C1–C4 correlate to the scintillating glasses [Colour available online]

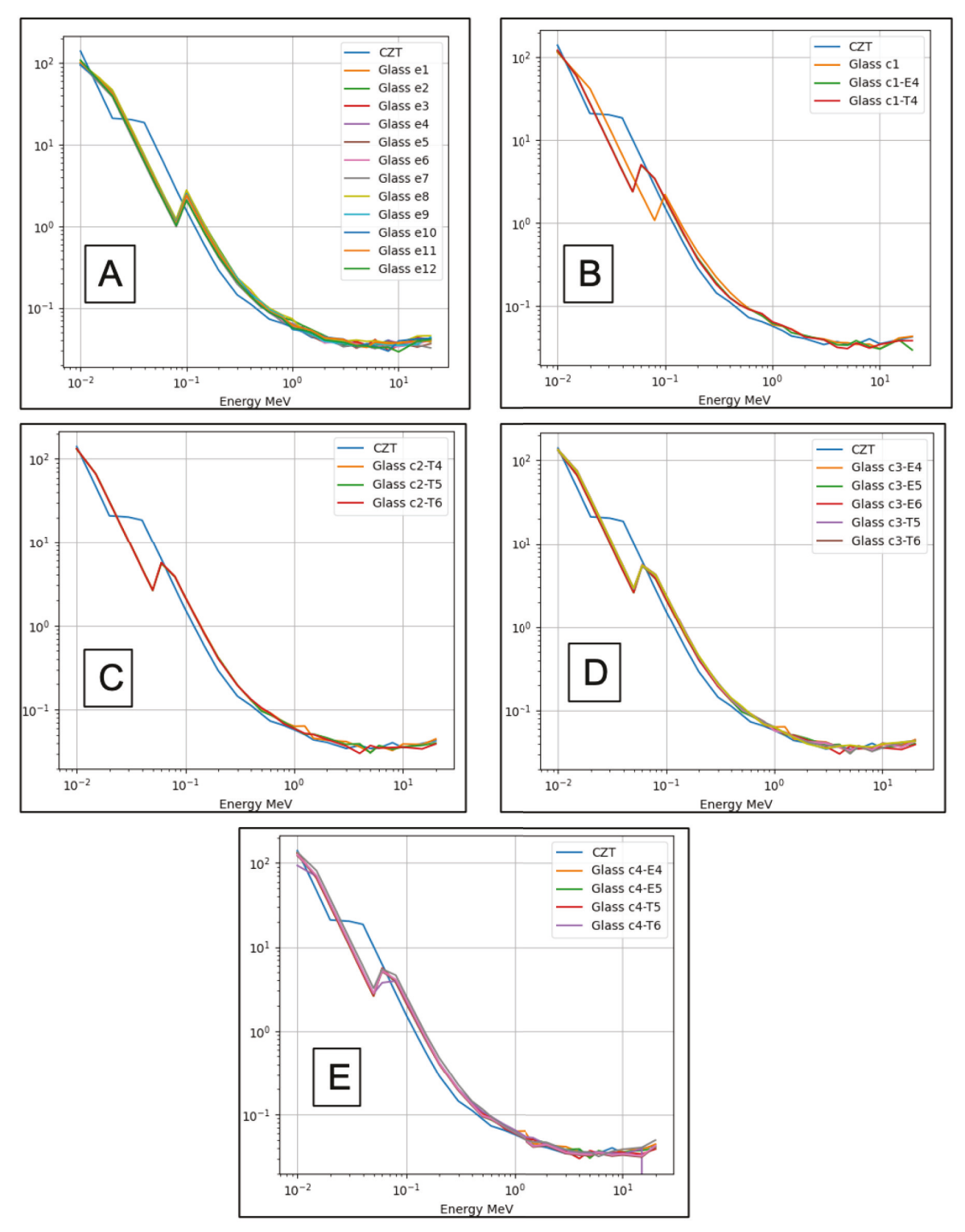


Figure 3. Mass attenuation of all glass samples compared to CZT. GATE simulations show that the glasses' mass attenuation coefficients are almost identical to CZT from about 0·1 MeV up to 20 MeV [Colour available online]

high lead concentration semiconducting glasses and high tungsten concentration scintillating glasses have comparable $Z_{\rm eff}$ values to that of CZT, which is 50. (37)

The $Z_{\rm eff}$ value is known to have energy dependency, and the power law is known to have its limitations. Consequently, the mass attenuation coefficients were also calculated. Mass attenuation coefficients, determined by GATE simulations, are displayed in Figure 3.

Based on our simulated data, both types of glasses

have slightly higher mass attenuation coefficients than CZT for energies below around 20 keV, corresponding to the range of molybdenum-based mammography. However, in the 20 to 60 keV energy range CZT mass attenuation coefficient is around two times higher than the tested glass samples. Beyond 60 keV (0.06 MeV) energy the mass attenuation coefficient values are almost the same for the glasses and CZT; this range corresponds to high-energy x-rays used in CT scans. (40)

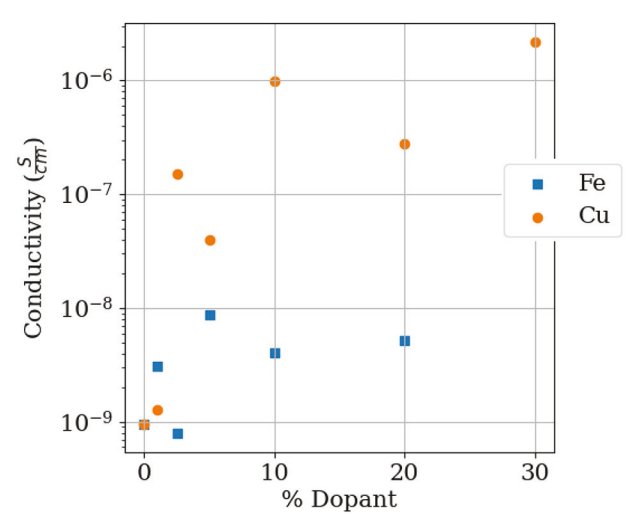


Figure 4. Conductivity measurements of semiconducting glasses, organized by dopant percentages and types. Blue squares are Fe-doped glasses, and orange circles represent the Cu-doped glass samples [Colour available online]

Based on the density data, varying the dopant concentrations would likely have an effect on mass attenuation. The scintillating glasses with increased dopant concentration and therefore increased density likely have higher mass attenuation coefficients than the values predicted for the base glasses. Inversely so with the semiconducting glasses, as the density decreased with increased dopant concentration.

The electrical conductivities of the semiconducting glasses are reported in Figure 4, in log scale, where an overall increase of the conductivity for higher dopant concentrations was observed. More specifically, increasing the concentration of copper increased the conductivity of the glasses by several orders of magnitude before mostly levelling off at 10 mol%. On the other hand, the effects of iron concentration on conductivity were relatively minor, with an overall conductivity increase by about an order of magnitude before seemingly levelling off immediately at 1 mol%. Conductivity at 2.5 mol% anomalously dropped below the conductivity of the base glass, while all samples with higher dopant concentrations seem to have conductivities consistent with the 1 mol% sample. It's unknown at this time why this anomaly is observed.

We propose two, non-exclusive, methods by which the change in conductivity with the addition of the dopants is brought about. The most obvious idea is dopants themselves could introduce new conduction mechanisms into the system. Transition metals in the form of transition metal oxides were originally chosen as dopants with this hypothesis in mind. The change in conductivity could also be brought about by a change in the valence state of V⁵⁺ to V⁴⁺ caused by the addition of transition metal dopants. (34) Indeed, the electrical conductivity of vanadate glasses is attributed to polaron hopping from V⁵⁺ to V⁴⁺ sites. (47)

The conductivity of CZT ranges from 10⁻⁸ to 10⁻⁹ S/cm for most compositions of CZT.⁽⁴⁸⁾ The iron-

Table 3. Europium ion photoluminescent transitions

Туре	Transition	Wavelength (nm)
Excitation	$^{7}F_{0} \rightarrow ^{5}D_{4}$	362
Excitation	${}^{7}F_0 \rightarrow {}^{5}G_2$	382
Excitation	${}^{7}F_0 \rightarrow {}^{5}L_6$	394
Excitation	$^{7}F_{1} \rightarrow ^{5}D_{3}$	414
Emission	$^{5}D_{0} \rightarrow ^{7}F_{0}$	579
Emission	$^{5}D_{0} \rightarrow ^{7}F_{1}$	591
Emission	$^{5}D_{0} \rightarrow ^{7}F_{2}$	613
Emission	$^{5}D_{0} \rightarrow ^{7}F_{3}$	652
Emission	$^{5}D_{0} \rightarrow ^{7}F_{4}$	701

doped samples fall within the range from 8.77×10^{-9} to 8.03×10^{-10} S/cm, very close to the conductivity range of CZT. The copper-doped samples, with the exception of the minimally doped 1 mol% sample, fall within a wide range from 2.15×10^{-6} to 3.96×10^{-8} S/cm, spanning from the upper bound of CZT conductivities and increasing by two orders of magnitude.

The photoluminescence spectra of the scintillating glasses are shown in Figure 5. Excitation spectra are presented on the left, while emission spectra are presented on the right. The top graphs correspond to the photoluminescence results from the europium-doped glasses, and the bottom ones are from the terbium-doped glasses.

For the europium doped samples, excitation peaks at 362, 382, 394 and 414 nm can be attributed to the ${}^7F_0 \rightarrow {}^5D_4$, ${}^7F_0 \rightarrow {}^5G_2$, ${}^7F_0 \rightarrow {}^5L_6$ and ${}^7F_1 \rightarrow {}^5D_3$ transitions of Eu³+ ions, respectively, and the emission peaks at 579, 591, 613, 652 and 701 nm can be attributed to the ${}^5D_0 \rightarrow {}^7F_0$, ${}^5D_0 \rightarrow {}^7F_1$, ${}^5D_0 \rightarrow {}^7F_2$, ${}^5D_0 \rightarrow {}^7F_3$ and ${}^5D_0 \rightarrow {}^7F_4$ transitions of Eu³+ ions, respectively. (43) For the terbium-doped samples, the excitation peaks at 352, 370 and 378 nm can be attributed to the ${}^7F_6 \rightarrow {}^5L_9$, ${}^7F_6 \rightarrow {}^5L_{10}$, and ${}^7F_6 \rightarrow {}^5G_6 + {}^5D_3$ of Tb³+ ions, respectively, and the emission peaks at 488, 544, 586 and 620 nm can be attributed to the ${}^5D_4 \rightarrow {}^7F_6$, ${}^5D_4 \rightarrow {}^7F_4$, ${}^5D_4 \rightarrow {}^7F_3$, transitions of Tb³+ ions, respectively. (19)

The europium excitation spectrum intensity is lowest at 1 mol% concentration and steadily increases intensity up to 5 mol%. At 6 mol% europium concentration, self-quenching effects dominate and intensity decreases appropriately. The europium emission spectrum behaves similarly. Emission intensity is lowest at 1 mol% and steadily increases up to 5 mol%. At 6 mol% concentration, emission intensity decreases due to self-quenching. The relative intensity of all excitation and emission peaks remains constant across the different dopant concentrations.

The terbium excitation spectrum intensity is lowest at 1 mol%. At 378 nm excitation, the highest intensity peak, all samples have similar intensity, with the 4 mol% sample being the most intense. At 370 nm ex-

Table 4. Terbium ion photoluminescent transitions

Туре	Transition	Wavelength (nm)
Excitation	$^{7}F_{6} \rightarrow ^{5}L_{9}$	352
Excitation	${}^{7}F_{6} \rightarrow {}^{5}L_{10}$	370
Excitation	${}^{7}F_{6} \rightarrow {}^{5}G_{6} + {}^{5}D_{3}$	378
Emission	$^{5}D_{4} \rightarrow ^{7}F_{6}$	488
Emission	$^{5}D_{4} \rightarrow ^{7}F_{5}$	544
Emission	$^{5}D_{4}\rightarrow ^{7}F_{4}$	586
Emission	$^{5}D_{4} \rightarrow ^{7}F_{3}$	620

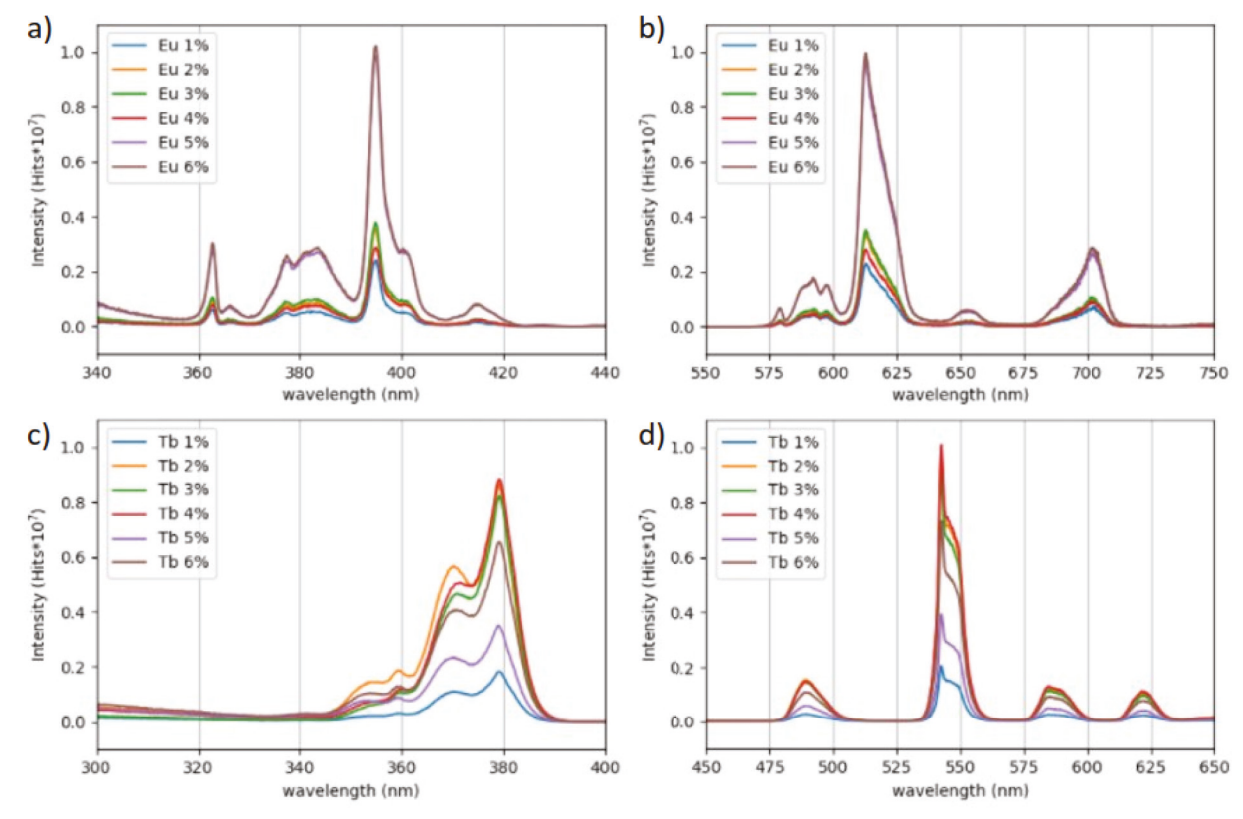


Figure 5. The photoluminescence excitation (a) and (c) and emission (b) and (d) spectra of the Eu- and Tb-doped scintillating glasses [Colour available online]

citation, the 3, 5 and 6 mol% samples all have similar intensity, however, this peak is more pronounced in the 2 and 4 mol% samples. The 352 nm excitation peak is the least pronounced, however, it is again anomalously prominent in the 2 mol% sample. The terbium emission spectrum intensity is lowest at 1 mol%. Emission spectrum intensity at 2, 3 and 5 mol% are all very similar. Emission spectrum intensity is the highest at 4 mol%. Self-quenching effects diminish the emission spectrum intensity at 6 mol%, making the spectrum intensity slightly lower than the 2, 3 and 5 mol% samples. The relative intensity of the emission peaks remains constant across the different dopant concentrations.

Conclusions

This work shows that scintillating and semiconducting glasses have the potential to be used as an active medium for x-ray detection. With a large density variation, from 4·5 to 6·3 g/cm³, choice of electrical or optical readout, and easy manufacturing these glasses have the potential to be used in a variety of applications.

All the semiconducting glasses and the scintillating glasses c1 and c2 are lacking in density when compared to CZT. However, the mass attenuation coefficients calculated from GATE simulations show that these glasses are comparable with CZT. The calculated mass attenuation coefficients predict that these glasses should interact with x-rays more intensely than CZT at energies lower than 20 keV, (45)

and that these glasses interact with x-rays nearly the same way for energies greater than 60 keV. (46)

This investigation also shows that increasing the dopant amount in the scintillating glass increases density. This could lead to higher mass attenuation coefficients and thereby even more effective detectors, though luminescence quenching effects may have to be considered.

Increasing the copper or iron dopant amount in the lead vanadate glasses causes a slight decrease in the density. This work shows that we can achieve three orders of magnitude variation in conductivities on these glasses, and this range can easily be extended. The high variability of the conductivities of these high-density glasses opens a vast range of applications areas from medical to space, to high-energy physics experiments.

The vanadium-based semiconducting glasses can be used in either high-energy physics or low-energy medical physics applications. Since CZT also is a semiconducting material, vanadium-based semiconducting glasses can easily replace CZT in the same detector systems.

In conclusion, this work showed potential for the use of either dense borate scintillating glasses or lead vanadate semiconducting glasses for the detection of x-rays.

Acknowledgments

This work was funded by Coe College, NSF-DMR 1746230, NSF-REU 1950337, R. J. McElroy Trust

Student/Faculty Research Fund. L.G. Jacobsohn acknowledges NSF-DMR 1653016.

References

- Ter-Pogossian, M. M. & Phelps, M. E. Semiconductor Detector Systems. Seminars Nucl. Med., 2006, 3 (4), 343–356.
- 2. Gruner, S. M. X-ray imaging detectors. Phys. Today, 2012, 65 (12), 29–34.
- Krawczynski, H. S., Stern, D., Harrison, F. A., Kislat, F. F., Zajczyk, A., Beilicke, M., Hoormann, J., Guo, Q., Endsley, R., Ingram, A. R., Miyasaka, H., Madsen, K. K., Aaron, K. M., Amini, R., Baring, M. G., Beheshtipour, B., Bodaghee, A., Booth, J., Borden, C., Böttcher, M., Christensen, F. E., Coppi, P. S., Cowsik, R., Davis, S., Dexter, J., Done, C., Dominguez, L. A., Ellison, D., English, R. J., Fabian, A. C., Falcone, A., Favretto, J. A., Fernández, R., Giommi, P., Grefenstette, B. W., Kara, E., Lee, C. H., Lyutikov, M., Maccarone, T., Matsumoto, H., McKinney, J., Mihara, T., Miller, J. M., Narayan, R., Natalucci, L., Özel, F., Pivovaroff, M. J., Pravdo, S., Psaltis, D., Okajima, T., Toma, K. & Zhang, W. W. X-ray polarimetry with the Polarization Spectroscopic Telescope Array (PolSTAR). Astropart. Phys., 2016, 75, 8–28.
- Roy, U. N., Camarda, G. S., Cui, Y., Gul, R., Yang, G., Zazvorka, J., Dedic, V., Franc, J. & James, R. B. Evaluation of CdZnTeSe as a highquality gamma-ray spectroscopic material with better compositional homogeneity and reduced defects. Sci. Rep., 2019, 9 (1), 7303.
- Schlesinger, T. E., Toney, J. E., Yoon, H., Lee, E. Y., Brunett, B. A., Franks, L. & James, R. B. Cadmium zinc telluride and its use as a nuclear radiation detector material. 2001, 32 (4–5), 103–189.
- Sordo, S. D., Abbene, L., Caroli, E., Mancini, A. M., Zappettini, A. & Ubertini, P. Progress in the development of CdTe and CdZnTe Semiconductor Radiation Detectors for Astrophysical and Medical Applications. Sensors (Basel), 2009, 9 (5), 3491–3526.
- Li, G., Zhang, X., Hua, H. & Jie, W. A Modified Vertical Bridgman Method for Growth of High-Quality Cd.(1-x)Zn.xTe Crystals. J. Electron. Mater., 2005, 34 (9), 1215–1224.
- Roy, U. N., Weiler, S., Stein, J., Hossain, A., Camarda, G. S., Bolotnikov, A. E. & James, R. B. Size and distribution of Te inclusions in THM asgrown CZT wafers: The effect of the rate of crystal cooling. *J. Cryst. Growth*, 2011, 332 (1), 34–38.
- Iniewski, K. CZT sensors for Computed Tomography: From crystal growth to image quality. J. Instrum., 2016, 11 (12), 12034.
- McCoy, J. J., Kakkireni, S., Gilvey, Z. H., Swain, S. K., Bolotnikov, A. E. & Lynn, K. G. Overcoming Mobility Lifetime Product Limitations in Vertical Bridgman Production of Cadmium Zinc Telluride Detectors. J. Electron. Mater., 2019, 48 (7), 4226–4234.
- Taki, Y., Shinozaki, K., Honma, T., Komatsu, T., Aleksandrov, L. & Iordanova, R. Coexistence of nano-scale phase separation and microscale surface crystallization in Gd₂O₃-WO₃-B₂O₃ glasses. *J. Non-Cryst.* Solids, 2013, 381, 17–22.
- Zhou, W., Martin, S. W., Schwellenbach, D. & Hauptman, J. New high-density fluoride glasses doped with CeF₃. J. Non-Cryst. Solids, 1995, 184, 84–92.
- Fu, J., Parker, J. M., Brown, R. M. & Flower, P.S. Compositional dependence of scintillation yield of glasses with high Gd₂O₃ concentrations.
 J. Non-Cryst. Solids, 2003, 326, 335–338.
- Wang, Q., Yang, B., Zhang, Y., Xia, H., Zhao, T. & Jiang, H. High light yield Ce³⁺-doped dense scintillating glasses. *J. Alloys Compd.*, 2013, 581, 801–804.
- Fu, J., Kobayashi, M., Sugimoto, S. & Parker, J. M. Eu³⁺-activated heavy scintillating glasses. *Mater. Res. Bull.*, 2008, 43 (6), 1502–1508.
- Pinto, I. C., Galleani G., Jacobsohn L. G., Ledemi Y., Messaddeq Y. & De Camargo, A. S. S. Fluorophosphate glasses doped with Eu³⁺ and Dy³⁺ for X-ray radiography. *J. Alloys Compd.*, 2021, 863, 158382.
- Jiang, J., Zhang, G. & Poulain, M. Cerium-containing glasses for fast scintillators. J. Alloys Compd., 1998, 275–277, 733–737.
- Hobson, P.R., Imrie, D. C., Price, T., Sheikh, S., Bell, K. W., Brown, R. M., Cockerill, D. J. A., Flower, P. S., Grayer, G. H., Kennedy, B. W., Lintern, A. L., Jeffreys, P. W., Sproston, M., Mckinlay, K. J., Parker, J. M., Bowen, D. L., Cliff, T., Stewart-Hannay, R. & Hammond-Smith, R. The development of dense scintillating hafnium fluoride glasses for the construction of homogeneous calorimeters in particle physics. J. Non-Cryst. Solids, 1997, 213&214, 147–151.
- Kilbourn, B. Lanthanide Oxides. Concise Encyclopedia of Advanced Ceramic Materials, 1991, 276–278.
- Nikl, M. Scintillation detectors for x-rays. Meas. Sci. Technol., 2016, 17, 37–54.
- Dahiya, M. S., Khasa, S., Yadav, A. & Agarwal, A. Appearance of small polaron hopping conduction in iron modified cobalt lithium bismuth borate glasses. AIP Conf. Proc., 2016, 1731, 70018.

- Barczynski, R. J., Gazda, M. & Murawski, L. Mixed ionic-polaron transport and rapid crystallization in (Bi,Pb)-Sr-Ca-Cu-O glass. Solid State Ion., 2003, 157 (1-4), 299–303.
- Rada, M., Rus, L., Rada, S., Pascuta, P., Stan, S., Dura, N., Rusu, T. & Culea, E. Role of vanadium ions on structural, optical and electrochemical properties of the vanadate-lead glasses. *J. Non-Cryst. Solids*, 2015, 414, 59–65.
- Mandal, S. & Ghosh, A. Electrical properties of lead vanadate glasses. *Phys. Rev. B*, 1994, 49 (5), 3131–3135.
- Wantana, N., Kaewnuam, E., Kim, H. J., Kang, S. C., Ruangtaweep, Y., Kothan, S. & Kaewkhao, J. X-ray/proton and photoluminescence behaviors of Sm³⁺ doped high-density tungsten gadolinium borate scintillating glass. *J. Alloys Compd.*, 2020, 849 (3), 156574.
- Kielty, M. W., Pan, L., Dettmann, M. A., Herrig, V.& Akgun, U., Jacobsohn, L. G. Luminescence of Ce-doped aluminophosphate glasses. J. Mater. Sci.: Mater. Electron., 2019, 30, 16774–16780.
- Schweizer, S. & Johnson, J. A. Fluorozirconate-based glass ceramic X-ray detectors for digital radiography. *Radiat. Meas.*, 2007, 42 (4–5), 632–637.
- 28. Xie, Q., Scheltzbaum, J. & Akgun, U. High density fluoride glass calorimeter. J. Instrum., 2014, 9 (4), 4001.
- 29. Tillman, I. J., Dettmann, M. A., Herrig, V., Thune, Z. L., Zieser, A. J., Michalek, S. F., Been, M. O., Martinez-Szewczyk, M. M., Koster, H. J., Wilkinson, C. J., Kielty, M. W., Jacobsohn, L. G. & Akgun, U. Highdensity scintillating glasses for a proton imaging detector. *Opt. Mater.*, 2017, 68, 58–62.
- Wilkinson, C. J., Goranson, K., Turney, A., Xie, Q., Tillman, I. J., Thune, Z. L., Dong, A., Pritchett, D., McInally, W., Potter, A., Wang, D. & Akgun, U. High density scintillating glass proton imaging detector. *Proc.* SPIE Med. Imaging 2017, Phys. Med. Imaging, 2017, 10132, 997–1005.
- Varney, G., Dema, C., Gul, B. E., Wilkinson, C. J. & Akgun, U. Use of Machine Learning in CARNA Proton Imager. *Proc. SPIE Med. Imaging* 2019, Phys. Med. Imaging, 2019, 10948, 1317–1325.
- Finneman, G., Meskell, N., Caplice, T., Eichhorn, O., Abu-Halawa, E., Stobb, M. & Akgun, U. Proton Imaging with Machine Learning. Proc. SPIE Med. Imaging 2021, Phys. Med. Imaging, 2021, 11595, 1338–1355.
- Ademoski, G. L., Simko, S., Teeple, M., Morrow, I., Kralik, P., Wilkinson, C. J., Varney, G., Martinez-Szewczyk, M., Yinong, L., Nimmagadda, J. K., Samant, S., Wu, Y., Pan, L., Jacobsohn, L. G., Wilkinson, Q., Duru, F. & Akgun, U. A glass neutron detector with machine learning capabilities. J. Instrum., 2019, 14 (6), 6013.
- Johnson, N., Wehr, G., Hoar, E., Xian, S., Akgun, U., Feller, S., Affatigato, M., Repond, J., Xia, L., Bilki, B. & Onel, Y. Electronically Conductive Vanadate Glasses for Resistive Plate Chamber Particle Detectors. *Int. J. Appl. Glass Sci.*, 2015, 6 (1), 26–33.
- Jan, S., Benoit, D., Becheva, E., Carlier, T., Cassol, F., Descourt, P., Frisson, T., Grevillot, L., Guigues, L., Maigne, L., Morel, C., Perrot, Y., Rehfeld, N., Sarrut, D., Schaart, D. R., Stute, S., Pietrzyk, U., Visvikis, D., Zahra, N. & Buvat, I. GATE V6: a major enhancement of the GATE simulation platform enabling modeling of CT and radiotherapy. *Phys. Med. Biol.*, 2011, 56 (4), 881–901.
- Sarrut, D., Bardiès, M., Boussion, N., Freud, N., Jan, S., Létang, JM., Loudos, G., Maigne, L., Marcatili, S., Mauxion, T., Papadimitroulas, P., Perrot, Y., Pietrzyk, U., Robert, C., Schaart, D. R., Visvikis, D. & Buvat, I. A review of the use and potential of the GATE Monte Carlo simulation code for radiation therapy and dosimetry applications. *Med. Phys.*, 2014, 41 (6), 64301.
- 37. Agostinelli, S., Allison, J., Amako, K., Apostolakis, J., Araujo, H., Arce, P., Asai, M., Axen, D., Banerjee, S., Barrand, G., Behner, F., Bellagamba, L., Boudreau, J., Broglia, L., Brunengo, A., Burkhardt, H., Chauvie, S., Chuma, J., Chytracek, R., Cooperman, G., Cosmo, G., Degtyarenko, P., Dell'Acqua, A., Depaola, G., Dietrich, D., Enami, R., Feliciello, A., Ferguson, C., Fesefeldt, H., Folger, G., Foppiano, F., Forti, A., Garelli, S., Giani, S., Giannitrapani, R., Gibin, D., Gómez Cadenas, J. J., González, I., Gracia Abril, G., Greeniaus, G., Greiner, W., Grichine, V., Grossheim, A., Guatelli, S., Gumplinger, P., Hamatsu, R., Hashimoto, K., Hasui, H., Heikkinen, A., Howard, A., Ivanchenko, V., Johnson, A., Jones, F. W., Kallenbach, J., Kanaya, N., Kawabata, M., Kawabata, Y., Kawaguti, M., Kelner, S., Kent, P., Kimura, A., Kodama, T., Kokoulin, R., Kossov, M., Kurashige, H., Lamanna, E., Lampén, T., Lara, V., Lefebure, V., Lei, F., Liendl, M., Lockman, W., Longo, F., Magni, S., Maire, M., Medernach, E., Minamimoto, K., Mora de Freitas, P., Morita, Y., Murakami, K., Nagamatu, M., Nartallo, P., Nieminen, R., Nishimura, T., Ohtsubo, K., Okamura, M., O'Neale, S., Oohata, Y., Paech, K., Perl, J., Pfeiffer, A., Pia, M. G., Ranjard, F., Rybin, A., Sadilov, S., Di Salvo, E., Santin, G., Sasaki, T., Savvas, N., Sawada, Y., Scherer, S., Sei, S., Sirotenko, V., Smith, D., Starkov, N., Stoecker, H., Sulkimo, J., Takahata, M., Tanaka, S., Tcherniaev, E., Safai Tehrani, E., Tropeano, M., Truscott, P., Uno, H., Urban, L., Urban, P., Verderi, M., Walkden, A., Wander, W., Weber, H., Wellisch, J. P., Wenaus, T.,

B. SMITH ET AL: SEMICONDUCTING AND SCINTILLATING GLASSES FOR X-RAY DETECTION

- Williams, D. C., Wright, D., Yamada, T., Yoshida, H., Zschiesche, D. Geant4 a simulation toolkit, *Nucl. Instrum. Methods A* 2003, **506**, 250.
- 38. Hubbell, J. H. & Seltzer, S. M. Tables of X-Ray Mass Attenuation Coefficients and Mass Energy-Absorption Coefficients from 1 keV to 20 MeV for Elements Z = 1 to 92 and 48 Additional Substances of Dosimetric Interest. *NIST SRD 126*, 1995.
- Lawaczeck, R., Arkadiev, V., Diekmann, F. & Krumrey, M. Monochromatic X-rays in Digital Mammography. *Investig. Radiol.*, 2005, 40 (1), 33–39.
- 40. Goo, H. W. & Goo, J. M. Dual-Energy CT: New Horizon in Medical Imaging. *Korean J. Radiol.*, 2017, **18** (4), 555–569.
- Rizzi, M., D'Aloia, M. & Castagnolo, B. Semiconductor Detectors and Principles of Radiation-matter Interaction. J. Appl. Sci., 2010, 10, 3141–3155.
- 42. Hayakawa, S., Yoko, T. & Sakka, S. IR and NMR structural studies on lead vanadate glasses. *J. Non-Cryst. Solids*, 1995, **183** (1–2), 73–84.
- 43. Wantana, N., Kaewnuam, E., Ruangtaweep, Y., Kidkhunthod, P., Kim,

- H. J., Kothan, S. & Kaewkhao, J. High-density tungsten gadolinium borate glasses doped with Eu³+ ion for photonic and scintillator applications. *Radiat. Phys. Chem.*, 2020, **172**, 108868.
- Yadav, A. K. & Singh, P.A review of the structures of oxide glasses by Raman spectroscopy. RSC Adv., 2015, 5 (83), 67583–67609.
- Lawaczeck, R., Arkadiev, V., Diekmann, F. & Krumrey, M. Monochromatic X-rays in Digital Mammography. *Investig. Radiol.* 2005, 40 (1), 33–39.
- Goo, H. W. & Goo, J. M. Dual-Energy CT: New Horizon in Medical Imaging. Korean J. Radiol., 2017, 18 (4), 555–569.
- Laila, S., Supardan S. N. & Yahya, A. K. Effect of ZnO addition and concurrent reduction of V₂O₅ on network formation and elastic properties of lead vanadate (55–x)V₂O₅–45PbO–(x)ZnO glass system. *J. Non-Cryst. Solids*, 2013, 367, 14–22
- Su C, Thermal conductivity, electrical conductivity, and thermoelectric properties of CdTe and Cd-0.8Zn-0.2Te crystals between room temperature and 780°C. AIP Advances, 2015, 5, 057118.